Impact of wall displacements on the large-scale flow coherence in ascending aorta

This article has been accepted for publication in the Journal of Biomechanics. This is the author's preprint version.
Citation information: DOI 10.1016/j.jbiomech.2023.111620

Impact of wall displacements on the large-scale flow coherence in ascending aorta

Karol Calò[1,2], Katia Capellini[3], Giuseppe De Nisco[1,2], Valentina Mazzi[1,2], Emanuele Gasparotti[3], Diego Gallo[1,2], Simona Celi[3], Umberto Morbiducci[1,2*]

1. Department of Mechanical and Aerospace Engineering, Politecnico di Torino, Turin, Italy
2. PoliTo[BIO]Med Lab, Politecnico di Torino, Turin, Italy
3. BioCardioLab, Bioengineering Unit - Heart Hospital, Fondazione Toscana "G. Monasterio", Massa, Italy

The final publication is available at: https://doi.org/10.1016/j.jbiomech.2023.111620

***Address for correspondence:**
Umberto Morbiducci, PhD
PoliTo[BIO]Med Lab
Department of Mechanical and Aerospace Engineering
Politecnico di Torino
Corso Duca degli Abruzzi, 24
10129 Turin, Italy
ORCID: 0000-0002-9854-1619
E-mail: umberto.morbiducci@polito.it

Abstract

In the context of aortic hemodynamics, uncertainties affecting blood flow simulations hamper their translational potential as supportive technology in clinics. Computational fluid dynamics (CFD) simulations under rigid-walls assumption are largely adopted, even though the aorta contributes markedly to the systemic compliance and is characterized by a complex motion. To account for personalized wall displacements in aortic hemodynamics simulations, the moving-boundary method (MBM) has been recently proposed as a computationally convenient strategy, although its implementation requires dynamic imaging acquisitions not always available in clinics.

In this study we aim to clarify the real need for introducing aortic wall displacements in CFD simulations to accurately capture the large-scale flow structures in the healthy human ascending aorta (AAo). To do that, the impact of wall displacements is analyzed using subject-specific models where two CFD simulations are performed imposing (1) rigid walls, and (2) personalized wall displacements adopting a MBM, integrating dynamic CT imaging and a mesh morphing technique based on radial basis functions. The impact of wall displacements on AAo hemodynamics is analyzed in terms of large-scale flow patterns of physiological significance, namely axial blood flow coherence (quantified applying the Complex Networks theory), secondary flows, helical flow and wall shear stress (WSS).

From the comparison with rigid-wall simulations, it emerges that wall displacements have a minor impact on the AAo large-scale axial flow, but they can affect secondary flows and WSS directional changes. Overall, helical flow topology is moderately affected by aortic wall displacements, whereas helicity intensity remains almost unchanged. We conclude that CFD simulations with rigid-wall assumption can be a valid approach to study large-scale aortic flows of physiological significance.

Keywords: computational fluid dynamics, flow coherence, aortic hemodynamics, helical flow, moving boundaries, wall shear stress

1. Introduction

The aorta is characterized by a remarkable hemodynamic richness in its thoracic segment, mainly dictated by proximity to the beating heart, aortic wall motion, and complex anatomy (Jin et al., 2003; Sengupta et al., 2008; Yearwood and Chandran, 1982). Such hemodynamic richness has contributed to make the aorta a site of election for fluid mechanics studies aimed at highlighting the links of blood transport with cardiovascular pathophysiology (Garcia et al., 2018; Guala et al., 2022; Markl et al., 2004; Morbiducci et al., 2011; Stokes et al., 2021; Vignali et al., 2021). At the same time, aortic hemodynamics is characterized by a large spatiotemporal heterogeneity that has contributed to hamper a robust, univocal definition of the large-scale coherent fluid structures characterizing normal aortic blood flow, and able to discriminate physiology from pathology (Calò et al., 2023).

In the last decades, the coupling of medical imaging and computational fluid dynamics (CFD) has gained momentum as an effective tool for studying the aortic hemodynamics with high spatiotemporal resolution in personalized in silico models (Antonuccio et al., 2021; Cilla et al., 2020; De Nisco et al., 2020; Gallo et al., 2012; Morbiducci et al., 2013; Romarowski et al., 2018). However, CFD models require assumptions which introduce important sources of uncertainty and might entail the generality of CFD-based results as well as their translation to clinics. In personalized CFD aortic models, a main source of uncertainty is represented by assumptions on wall displacements. In this regard, a largely adopted model idealization is the rigid-wall assumption, even if some studies suggest that incorporating MRI-measured subject-specific wall displacements into CFD simulations provides better agreement in terms of velocity fields with in vivo observations (Jin et al., 2003; Lantz et al., 2014). Two approaches alternative to rigid-wall CFD simulations can be implemented to account for aortic wall displacements. The first one is based on the classical fluid-structure interaction (FSI) modelling strategy (Caballero and Laín, 2015; Mirramezani and Shadden, 2022). However, FSI requires additional assumptions on wall material properties, which cannot be easily determined in vivo and therefore represent further sources of uncertainty. Moreover, FSI is characterized by an increased complexity and computational efforts hindering its clinical translation. To overcome FSI inherent limitations, an alternative approach based on the moving-boundary method (MBM) has emerged. MBM relies on the integration of clinical image-based measurements of wall displacements along the cardiac cycle and CFD simulations in the same computational framework (Capellini et al., 2020; Lantz et al., 2019; Torii et al., 2010), allowing to incorporate subject-specific wall displacements in simulations at lower computational costs and without posing any hypothesis on vessels wall material properties. Among the MBM strategies applied to in silico aortic models (Bonfanti et al., 2018; Jin et al., 2003; Lantz et al., 2014; Stokes et al., 2021), a framework integrating dynamic CT images, transient CFD simulations and a mesh morphing technique based on Radial Basis Functions (RBF) was recently introduced (Capellini et al., 2020). The RBF-based mesh morphing strategy has the advantage of keeping mesh connectivity avoiding re-meshing at each time-step of the simulation, which would result in a considerable increase in computational time. Moreover, the RBF-based morphing strategy has proven its capability in reproducing large deformations like those characterizing ascending thoracic aortic aneurysm progression, while preserving mesh quality (Biancolini et al., 2020; Capellini et al., 2018).

The overarching hypothesis of this study is that wall displacements might impact the coherence of large-scale blood flow structures in the ascending aorta (AAo) in such a way that might not be accounted for assuming rigid-walls in aortic CFD simulations. Interpreting the large-scale AAo hemodynamics in terms of flow coherence finds its rationale in the effectiveness of a coherence-based analysis in characterizing physiologically relevant conditions such as flow recirculation, separation and reattachment, local heterogeneity in the flow field, and mechanisms governing stirring and mixing (Shadden and Taylor, 2008). The above-mentioned hypothesis is tested on three subject-specific models of healthy human thoracic aorta performing two simulations on each reconstructed anatomy, assuming: (1) aortic rigid-walls, and (2) subject-specific aortic wall displacements imposed applying an RBF-based mesh morphing strategy (Capellini et al., 2020). The influence of wall displacements on the AAo large-scale fluid structures is analyzed in terms of through-plane velocity coherence and in-plane velocity distribution, as well as in terms of helical flow because of its recognized physiological significance in cardiovascular flows (Liu et al., 2009; Morbiducci et al., 2011). For the sake of completeness, the study is complemented by the analysis of the impact that aortic wall displacements have on wall shear stress (WSS), given its established role in the initiation and progression of vascular disease.

2. Materials and methods

An overview of the here adopted methods is provided in the schematic diagram in Fig. 1. Three male subjects of 25, 89 and 64 years old respectively were retrospectively selected and analyzed for this study. The three patients were affected by cardiac diseases, but they did not present aneurysmatic or aortic valve pathologies. A 320-detector scanner (Toshiba Aquilon One, Toshiba, Japan) was used to acquire dynamic CT scans of the aorta at 10 ECG-gated phases of the cardiac cycle. At each acquired phase, the 3D geometry of the AAo, arch and supra-aortic vessels was reconstructed within the VMTK (www.vmtk.org) environment. Details on image processing and geometries reconstruction, extensively described in previous studies (Capellini et al., 2020, 2018), are reported in the Supplementary Material.

2.1 Computational hemodynamics

On each subject two different modelling strategies were adopted: (1) CFD simulation assuming aortic rigid walls, performed on the geometry reconstructed from CT images acquired at the 0% phase of the cardiac cycle; (2) CFD simulation with aortic wall displacements along the cardiac cycle imposed by applying an RBF mesh morphing on the 10 reconstructed transient anatomies of the aorta (Capellini et al., 2020, 2018) (Fig. 1). The same computational settings and boundary conditions were adopted in the rigid- and the moving-wall CFD simulations. Briefly, aortic blood was assumed an incompressible, homogeneous, Newtonian fluid (density ρ =1060 kg m^{-3},

This article has been accepted for publication in the Journal of Biomechanics. This is the author's preprint version.
Citation information: DOI 10.1016/j.jbiomech.2023.111620

dynamic viscosity μ=0.0035 Pa s). The governing Navier-Stokes equations of fluid motion were solved in their discrete form using the finite volume-based CFD code Fluent (ANSYS Inc., USA) on computational grids consisting of tetrahedral elements in the lumen region and four layers of triangular prisms in the near-wall region. Echocardiographic velocity measurements were used to derive individualized inflow boundary conditions. Boundary conditions at the supra-aortic and at the descending aorta (DAo) outflow sections were set adopting a 3D-0D coupling approach through the implementation of lumped three-elements Windkessel models (Fig. 1). Details on the strategy implemented to prescribe boundary conditions are reported in the Supplementary Material.

In CFD simulations where wall displacements were imposed, a scheme proposed elsewhere (Capellini et al. 2020, 2018) was applied. Briefly, CFD is integrated with a morphing technique based on the aortic geometries reconstructed along the cardiac cycle from dynamic CT recordings thus imparting subject-specific aortic wall displacements without re-meshing adopting an RBF anatomic basis of representation. As the method only relies on the knowledge of wall displacements at different phases along the cardiac cycle, no assumption on the vessels' material properties was introduced. Descriptive notes on the RBF mesh-morphing technique are briefly reported in the Supplementary Material. For both the rigid- and moving-wall simulations, a no-slip condition was applied to the wall. To ensure that CFD solutions were not affected by initial transients, three cardiac cycles were simulated and the results relative to the third cycle were considered.

2.2 Large-scale hemodynamics characterization in the ascending aorta

This study analyzed the impact of aortic wall motion on the spatiotemporal heterogeneity of the large-scale fluid structures in the AAo. The aortic hemodynamics was characterized in terms of axial (through-plane) V_{ax} and secondary V_{sc} (in-plane) blood velocity components, obtained by projecting the local blood velocity vector **V** along the direction of the local vessel centerline and on the local transversal plane, respectively (Fig. 1), as extensively proposed elsewhere (Calò et al., 2021, 2020; Morbiducci et al., 2015). The sign of V_{ax} is representative of the main flow direction (positive, forward flow; negative, retrograde flow), whereas V_{sc} is related to aortic secondary flow structures (on the vessel's cross-section).

Given the well-established physiological significance of helical flow in arteries (Liu et al., 2015; Stonebridge et al., 2016) and in particular in aorta (Kilner et al., 1993; Morbiducci et al., 2011, 2009), the large-scale intravascular aortic hemodynamics was also characterized in terms of kinetic helicity density H_k, defined as the internal product of the velocity vector $\mathbf{V}$ with the vorticity vector $\boldsymbol{\omega}$ (Fig. 1). H_k is a pseudoscalar quantity with its sign indicating the direction of rotation of the helical flow structures (positive, right-handed; negative, left-handed). Here H_k was normalized to obtain the Local Normalized Helicity (LNH, Fig. 1), which has been demonstrated to be effective in visualizing helical flow patterns in arteries (Morbiducci et al., 2013, 2007). Furthermore, established helicity-based quantities (Fig. 1) evaluating the amount, intensity and topological features of helical flow structures were also computed (Morbiducci et al., 2013): h_1 and h_2, measuring the average net amount and intensity of helical flow over the cardiac cycle, respectively; h_3, an indicator of the presence of balanced/unbalanced counter-rotating helical flow patterns.

To evaluate the impact of wall displacements on the spatiotemporal coherence of the large-scale structures characterizing the AAo hemodynamics, a correlation-based analysis was performed. In detail, the similarity in shape between the simulated waveforms of the hemodynamic quantities (HQs) along the cardiac cycle at corresponding nodes *i* of the computational grid of the rigid- and moving-wall models was measured using the pairwise Pearson correlation coefficient $\mathrm{R}_{HQ,i}^{R-M}$ (Fig. 1).

The effect of the aortic wall displacements was also investigated analyzing the similarity of the large-scale axial flow features in AAo as described by V_{ax} waveforms along the cardiac cycle with the subject-specific blood flow rate waveform at the AAo inlet section, here considered as a main driving factor conditioning the dominant aortic hemodynamics in healthy subjects. To do that, a scheme based on complex networks theory was adopted and for each subject two *"one-to-all"* networks (one for the rigid- and one for the moving-wall model) were built (Fig. 1), as proposed elsewhere (Calò et al., 2023, 2020). By construction the *"one-to-all"* network contains a reference

This article has been accepted for publication in the Journal of Biomechanics. This is the author's preprint version.
Citation information: DOI 10.1016/j.jbiomech.2023.111620

node represented by the subject-specific blood flow rate waveform $Q(t)$, with the remaining nodes represented by the $V_{ax,i}(t)$ waveforms as obtained from the rigid- or moving-wall CFD simulations and defined at each mesh grid point *i* of the AAo. To characterize the relationship between the driving flow rate waveform and axial blood flow, the links of the network were weighted by the Pearson correlation coefficient between $Q(t)$ and each $V_{ax,i}(t)$ waveform, and the anatomical length of persistence of the $Q(t) - V_{ax}(t)$ correlation in AAo was quantified computing the *Average Weighted Curvilinear Distance* ($AWCD$) network metric, defined as (Calò et al., 2023):

$$AWCD = \frac{1}{l}\frac{1}{N}\sum_{i=1}^{N} \mathrm{R}_{Q,i}\, s_i, \qquad (2)$$

where *l* is the centerline's length of the AAo segment, *N* is the number of nodes, $\mathrm{R}_{Q,i}$ is the correlation coefficient between $Q(t)$ and the $V_{ax,i}(t)$ waveform at node *i*, and s_i is the curvilinear distance between the AAo inflow section (where the reference node is located by construction) and the vessel cross-section where node *i* is located (Fig. 1). By measuring the length of persistence of the $Q(t) - V_{ax}(t)$ waveforms correlation along the *"one-to-all"* network links in AAo, $AWCD$ provides a quantification of the sphere of influence of the aortic flow rate waveform on the distal large-scale axial flow structures (Calò et al., 2023).

2.3 Wall shear stress in the ascending aorta

The effect of AAo wall displacements on WSS was quantified in terms of the two canonical quantities time-averaged WSS (TAWSS, measuring the local average value of WSS magnitude along the cardiac cycle; Table 1) and oscillatory shear index (OSI, a measure of WSS directional changes along the cardiac cycle; Table 1), as well as the recently proposed topological shear variation index (TSVI, quantifying the variability in the contraction/expansion action exerted by the WSS on the endothelium along the cardiac cycle (De Nisco et al., 2020; Mazzi et al., 2021); Table 1).

3. Results

The AAo geometries at 5 representative phases of the cardiac cycle are shown in Fig. S1 of the Supplementary Material.

3.1 Impact of aortic motion on the large-scale axial flow

The volumetric maps of the correlation coefficients $\mathrm{R}_{V_{ax,i}}^{R-M}$ between the $V_{ax,i}(t)$ waveforms at corresponding nodes of the rigid- and moving-wall models are presented in Fig. 2. Overall, it emerges that the large-scale axial velocity waveforms along the cardiac cycle in the rigid- and in the moving-wall aorta are strongly correlated in all the analyzed subjects (Table S2 in the Supplementary Material), particularly in the bulk of the proximal AAo and in the entire AAo distal portion (Fig. 2). The observed moderate loss of correlation between axial flow patterns ($\mathrm{R}_{V_{ax,i}}^{R-M} < 0.8$) in the rigid- and moving-wall models is restricted to the near-wall regions of the aortic root and of the proximal AAo (Fig. 2).

The results of the *"one-to-all"* network analysis are presented in Fig. 3 in terms of volumetric maps of the correlation coefficients between $Q(t)$ and $V_{ax,i}(t)$ waveforms in the rigid- ($\mathrm{R}_{Q,i}^{R}$) and in the moving-wall ($\mathrm{R}_{Q,i}^{M}$) models. Consistently with the results in Fig.2, $\mathrm{R}_{Q,i}^{R}$ and $\mathrm{R}_{Q,i}^{M}$ distributions are similar for all the investigated subjects. In general, the results of Fig. 3 suggest that the flow rate waveform $Q(t)$ entering the AAo markedly shapes $V_{ax}(t)$ waveforms in the bulk of both rigid- and moving-wall models (as proven by the high correlation values, Table S3 in the Supplementary Material), while the similarity is partially lost in the near-wall region of the aortic root and of mid AAo. Interesting findings emerge from the calculation of the anatomical length of persistence of the correlation between the subject-specific blood flow rate and the large-scale axial flow structures, which overall varies from the 42% to 45% of the total length (l) of the AAo for all subjects, with a 4.4% maximum $AWCD$ percentage difference between rigid- and moving-wall models (in subject S2), as highlighted by the $AWCD$ values reported in Fig. 3.

3.2 Impact of aortic motion on secondary flows

A picture of the secondary flows establishing in the rigid- and moving-wall aortic models is depicted in Fig. 4, where the volumetric maps of $|V_{sc}|$, cycle-averaged as well as at three different phases of the cardiac cycle (peak systole, maximum flow acceleration and deceleration), are presented for the explanatory subject S1 together with the secondary flow patterns over three cross-sections of the AAo (results for subjects S2 and S3 are reported in the Supplementary Material). Overall, discernible differences emerge between the spatiotemporal organization of secondary flows in the rigid-wall model and the moving-wall one (Fig.4). This is evident from the cross-sectional maps, highlighting how AAo wall displacements affect the topology of secondary flows, causing in-plane vortex structures dislocation, stretching but also formation, compared to the rigid-wall model (see cross-sections in Fig.4).

The impact of wall displacements on AAo hemodynamics is further analyzed in terms of ratio $|V_{sc}|/|V_{ax}|$ of the local in-plane and through-plane velocity components magnitude values. The boxplots in Fig. 5 compare the rigid- and moving-wall models in terms of distributions of $|V_{sc}|/|V_{ax}|$ values, averaged along the cardiac cycle and at three phases of the cardiac cycle, and at three AAo cross-sections for all the analyzed subjects (the corresponding $|V_{sc}|/|V_{ax}|$ surface maps are reported in the Supplementary Material): at maximum flow acceleration and at peak systole axial velocity is the dominant velocity component ($|V_{sc}|/|V_{ax}|$<0.4, Fig. 5), independent of wall displacement, in all the subjects; the amount of secondary flows increases at maximum flow deceleration, but with a higher variability (in particular in subjects S1 and S3), highlighting that in certain locations V_{sc} equals or predominates over V_{ax} ($|V_{sc}|/|V_{ax}|$>1.0, Fig. 5). Around maximum flow deceleration, in general $|V_{sc}|/|V_{ax}|$ is higher in the moving-wall models than in the rigid ones. All this reflects on the cycle-average data, highlighting the higher contribution of V_{ax} to the aortic velocity vector field (Fig. 5).

3.3 Impact of aortic motion on helical flow

The volumetric maps of the pairwise correlation coefficients $\mathrm{R}_{H_{k,i}}^{R-M}$ measuring the spatiotemporal similarity of helical flow in the rigid- and moving-wall models are displayed in Fig. 6. Overall, it emerges that the kinetic helicity density waveforms along the cardiac cycle in the rigid-and moving-wall models are weakly-to-moderately correlated positively, with $\mathrm{R}_{H_{k,i}}^{R-M}$ value distributions characterized by marked variability in all the analyzed subjects (Table S4 in the Supplementary Material). The negative high-magnitude $\mathrm{R}_{H_{k,i}}^{R-M}$ values indicate the presence of aortic regions where $H_{k,i}(t)$ waveforms obtained from the rigid- and moving-wall simulations are opposite in phase (Fig. 6), i.e., they present similar temporal variations but with opposite H_k signs, or in other words opposite directions of rotation of the helical blood flow patterns (Fig.1).

The volumetric maps of LNH averaged along the cardiac cycle are adopted to visualize helical flow topological features in AAo (Fig. 7). Independent of the subject, two distinguishable coherent counter-rotating helical flow structures (left-handed, blue color; right-handed, red color) characterize the hemodynamics of both rigid- and moving-wall models, but with some differences in the cycle-average LNH profiles on the AAo cross-sections (Fig. 7). In detail, in S1 rigid-wall model the two counter-rotating helical fluid structures are overall balanced, whereas the moving-wall model is characterized by a larger right-handed helical structure developing from the mid to the distal AAo. In the other two subjects, while changing the topology of helical structures compared to the rigid-wall model, the moving-wall does not markedly affect the balance (in subject S3) or unbalance (in subject S2) of the two counter-rotating helical structures (Fig. 7).

These qualitative observations are quantitatively confirmed by the helicity-based quantities (Table 2). In particular, the negative (low in magnitude) h_1 and h_3 values for subject S2 indicate a slight predominance of a left-handed helical structure both in the rigid- and the moving-wall model, whereas the close-to-zero h_1 and h_3 values in subject S3 are indicative of an overall rotational balance. The difference in h_1 values between rigid- and moving-wall models in S1 (0.15 *vs.* 0.46 m s^{-2}, respectively) reflects a minimal effect of wall motion on the (close to zero) average net amount of helical flow over the cardiac cycle, with a slight predominance of a right-handed helical structure (positive h_1 values) in this subject. In fact, in terms of fluid mechanics the observed difference in h_1 values indicates that in the moving-wall model a small amount of helical flow patterns reversed their direction of rotation from left-handed to right-handed, compared to the rigid-wall model (Fig. 7), thus contributing to a higher positive h_1 value. However, this effect is not relevant, if we look at the corresponding values of helicity intensity h_2 (Table 2). Moreover, the positively low value of h_3 (0.12) in the S1 moving-wall model confirms the presence of the more (even if moderately) pronounced right-handed helical structure, which is balanced by a left-handed one of similar strength (h_3 closer to 0) in the rigid-wall model (Table 2, Fig. 7). Unlike helical flow topology, the intensity of helical flow undergoes only moderate variation due to wall displacements, as proven by the similar h_2 values characterizing the helical flow in rigid- and moving-wall models (Table 2).

3.4 Impact of aortic motion on wall shear stress

The impact of wall displacements on AAo hemodynamics is analyzed also comparing the distributions of the WSS-based quantities. For each subject, TAWSS and TSVI present very similar distributions on the luminal surface of the rigid- and of the moving-wall model, while more marked differences characterize OSI distributions (Fig. 8). The analysis of the scatter plots in Fig. 8 confirms that assuming rigid aortic walls has a more marked impact on OSI (rigid- *vs.* moving-wall correlation coefficients R in the range 0.43-0.54) than on TAWSS and TSVI (rigid- *vs.* moving-wall correlation coefficients R in the range 0.83-0.90 for TAWSS, and in the range 0.89-0.94 for TSVI).

4. Discussion

In the context of uncertainty quantification in computational hemodynamics, the real need for incorporating aortic wall displacements in simulations is still debated. Even though standard CFD simulations of the aortic hemodynamics are based on the rigid-wall assumption, previous studies reported that incorporating aortic wall displacements in aortic flow computer models has allowed to obtain e.g. (1) velocity fields closer to in vivo measurements (Jin et al., 2003; Lantz et al., 2014), (2) distributions of WSS-based quantities on the luminal surface similar to rigid-wall CFD simulations but with different local values (Reymond et al., 2013; Stokes et al., 2021), and (3) comparable integral values of helicity intensity (Capellini et al., 2020). To date, the impact of wall displacements on AAo blood flow organization has not been explored.

By using an RBF-based mesh morphing strategy to reproduce subject-specific wall motion, this study investigates the impact of wall displacements on the large-scale hemodynamics in the AAo, analyzing the modifications (1) in the persistence of similarity of fluid structures along the main flow direction, (2) in the structure of secondary flows, (3) in helical flow, given by the composition of axial and secondary flow, and (4) in WSS profiles. The AAo was selected for the analysis because it is site of election of a relevant portion of pathologies affecting the aorta (Ellozy, 2017; LeMaire and Russell, 2011; Thiene et al., 2021); in addition to that, it was recently found that the persistence of similarity of large-scale flow structures is maintained up to the distal AAo, in healthy subjects (Calò et al., 2023). The final aims of this study were: (1) identifying the mechanistic role of wall displacements in shaping large-scale hemodynamics in AAo, quantifying their impact on axial and secondary flows; (2) evaluating the overall impact of aortic wall displacements on helical flow (given by the composition of axial and secondary flows) and WSS profiles, because of their demonstrated physiological significance (Liu et al., 2009; Morbiducci et al., 2011); (3) clarifying if rigid-wall CFD simulations satisfactorily capture large-scale fluid structures in the AAo.

Among the main results it emerged that aortic wall displacements have small impact when considering axial blood flow: except for a narrow near-wall region in the aortic root, $V_{ax,i}(t)$ waveforms in the rigid- and moving-wall models are strongly correlated (median value above 0.96, Fig. 2 and Table S2). Consistently, the negligible differences in $AWCD$ values (lower than 4.5%, Fig. 3) between rigid- and moving-wall simulations suggest that rigid-wall simulations accurately replicate the anatomical length of persistence of the correlation of the axial blood flow along the AAo. By exploiting the network formalism and adopting the definition of flow coherence as imparted by the driving action of the proximal AAo blood flow rate waveform, the *"one-to-all"* approach adds the quantitative information on the length of persistence of the similarity with a driving flow rate waveform in the AAo large scale hemodynamics (Calò et al., 2023).

Different from the large-scale axial flow, wall displacements impact more markedly secondary flow patterns (Fig. 4, Fig. S1 and Fig. S2). This observation is confirmed by the analysis of the spatial distributions of the $|V_{sc}|/|V_{ax}|$ ratio in AAo: even though V_{ax} provides the major contribution to the aortic velocity vector field (in line with previous findings, see Jin et al., 2003) independent of aortic wall displacement, differences emerge between rigid- and moving-wall simulations (Fig. 5).

The changes in secondary flow patterns imparted by wall displacements in AAo reflect only moderately on helical flow. From rigid- and moving-wall simulations marginal differences emerge in the cycle-average net amount of helical flow as measured by h_1 and in helicity intensity h_2 (Table 2), suggesting that the overall impact of wall displacement on secondary flows affects helical flow topology modestly (as expressed in terms of H_k waveforms similarity, Fig. 6, and LNH distributions, Fig. 7) and its intensity marginally, in AAo. This finding suggests that helical flow intensity h_2, which has been demonstrated to play an atheroprotective role in arteries by suppressing flow distortions (Gallo et al., 2018; Morbiducci et al., 2011, 2009), could be affordably quantified with CFD simulations adopting the rigid-wall assumption.

Regarding WSS, it emerged that AAo wall displacements have no marked impact on the distributions on the luminal surface of the cycle-average WSS magnitude (TAWSS) and on the variability of the WSS contraction/expansion action along the cardiac cycle (TSVI) (Fig. 8). More marked differences emerged for OSI, with rigid-walls assumption leading to a moderate underestimation (Fig. 8), in agreement with previous findings (Capellini et al., 2020; Stokes et al., 2021) suggesting an impact of aortic wall displacements on WSS direction reversal along the cardiac cycle.

Some limitations could weaken the findings of this study. The first one is the application of an idealized flat velocity profile as boundary condition at the inlet. As suggested in previous studies, fully personalized inflow boundary conditions should be applied to realistically model aortic hemodynamics (Morbiducci et al., 2013; Youssefi et al., 2018). However, the idealization introduced here to manage inflow boundary conditions marginally entails the generalization of our findings, which are related to the sole effect of aortic wall motion on large-scale flow coherence. In this sense, applying the same boundary conditions to rigid- and moving-wall models allowed to relate the observed differences to univocal causes.

In this study only 10 phases of ECG-gated CT scans were acquired and, consequently, the wall displacements were available only for a limited percentage of the cardiac cycle. Although the temporal resolution of the acquired dynamic CT images is limited compared to more dynamic modalities such as echo and magnetic resonance, advantages associated to CT imaging in terms of spatial resolution should be considered.

Another limitation is represented by the assumption of Newtonian rheological behavior for blood. However, the choice of blood rheological models in aorta is still an open point of discussion (Menut et al., 2018). Lastly, only three subjects were analyzed in this study, therefore further investigations with larger datasets are needed to confirm the present findings.

Finally, the herein simulated hemodynamics does not account for turbulent phenomena that may occur also in healthy aortas. However, this modelling assumption does not entail the generality of the results because the focus of the study is on large-scale aortic fluid structures.

5. Conclusions

In this study the impact of aortic wall displacements on the coherence of the large-scale fluid structures in AAo was investigated by integration of in vivo measurements with an RBF-based mesh morphing strategy, and CFD. The comparative analysis of the results from rigid- and moving-wall simulations suggests that aortic wall displacements might impact secondary flows topology but not the large-scale axial flow. Moreover, the structure of secondary flows when considering wall displacements contribute to establish helical flow patterns in AAo with modest topological differences compared to rigid-wall models, whereas helicity intensity is not significantly affected.

Hence, the findings of this study suggest that the rigid-wall assumption might be a satisfactory approximation when modelling the aortic hemodynamics to investigate the large-scale spatiotemporal coherence of axial flow (Calò et al., 2023, 2021) or helical flow profiles as indicators of physiological significance (Gulan et al., 2014; Liu et al., 2015; Morbiducci et al., 2011, 2009; Oechtering et al., 2020). Considering the increased complexity and computational efforts required by moving-wall simulations, especially when adopting FSI, the hemodynamic picture provided by rigid-wall aortic models might still be considered reasonable in the context of potential clinical practicality (Brown et al., 2012).

Conflict of interest statement

The authors state no conflict of interest for the study object of the manuscript. The research was not supported financially by private companies. None of the authors has a financial agreement with peoples or organizations that could inappropriately influence their work.

Acknowledgments

KC, GDN, VM, DG and UM have been supported by MIUR FISR—FISR2019_03221 CECOMES.

References

Antonuccio, M.N., Mariotti, A., Fanni, B.M., Capellini, K., Capelli, C., Sauvage, E., Celi, S., 2021. Effects of Uncertainty of Outlet Boundary Conditions in a Patient-Specific Case of Aortic Coarctation. Annals of Biomedical Engineering 49, 3494–3507.

Biancolini, M.E., Capellini, K., Costa, E., Groth, C., Celi, S., 2020. Fast interactive CFD evaluation of hemodynamics assisted by RBF mesh morphing and reduced order models: the case of aTAA modelling. International Journal on Interactive Design and Manufacturing (IJIDeM) 14, 1227–1238.

Bonfanti, M., Balabani, S., Alimohammadi, M., Agu, O., Homer-Vanniasinkam, S., Díaz-Zuccarini, V., 2018. A simplified method to account for wall motion in patient-specific blood flow simulations of aortic dissection: Comparison with fluid-structure interaction. Medical Engineering & Physics 58, 72–79.

Caballero, A.D., Laín, S., 2015. Numerical simulation of non-Newtonian blood flow dynamics in human thoracic aorta. Computer Methods in Biomechanics and Biomedical Engineering 18, 1200–1216.

Calò, K., Gallo, D., Guala, A., Rizzini, M.L., Dux-Santoy, L., Rodriguez-Palomares, J., Scarsoglio, S., Ridolfi, L., Morbiducci, U., 2023. Network-Based Characterization of Blood Large-Scale Coherent Motion in the Healthy Human Aorta With 4D Flow MRI. IEEE Transactions on Biomedical Engineering 70, 1095–1104.

Calò, K., Gallo, D., Guala, A., Rodriguez Palomares, J., Scarsoglio, S., Ridolfi, L., Morbiducci, U., 2021. Combining 4D Flow MRI and Complex Networks Theory to Characterize the Hemodynamic Heterogeneity in Dilated and Non-dilated Human Ascending Aortas. Annals of biomedical engineering 49, 2441–2453.

Calò, K., Gallo, D., Steinman, D.A., Mazzi, V., Scarsoglio, S., Ridolfi, L., Morbiducci, U., 2020. Spatiotemporal Hemodynamic Complexity in Carotid Arteries: an Integrated Computational Hemodynamics & Complex Networks-Based Approach. IEEE Transactions on Biomedical Engineering 67, 1841–1853.

Capellini, K., Gasparotti, E., Cella, U., Costa, E., Fanni, B.M., Groth, C., Porziani, S., Biancolini, M.E., Celi, S., 2020. A novel formulation for the study of the ascending aortic fluid dynamics with in vivo data. Medical Engineering & Physics 91, 68–78.

Capellini, K., Vignali, E., Costa, E., Gasparotti, E., Biancolini, M.E., Landini, L., Positano, V., Celi, S., 2018. Computational Fluid Dynamic Study for aTAA Hemodynamics: An Integrated Image-Based and Radial Basis Functions Mesh Morphing Approach. Journal of Biomechanical

Engineering 140, 118–124.

Cilla, M., Casales, M., Peña, E., Martínez, M.A., Malvè, M., 2020. A parametric model for studying the aorta hemodynamics by means of the computational fluid dynamics. Journal of Biomechanics 103, 109691.

De Nisco, G., Tasso, P., Calò, K., Mazzi, V., Gallo, D., Condemi, F., Farzaneh, S., Avril, S., Morbiducci, U., 2020. Deciphering ascending thoracic aortic aneurysm hemodynamics in relation to biomechanical properties. Medical engineering & physics 82, 119–129.

Ellozy, S., 2017. Classification of aortic pathologies. Endovasc Today 16, 36–38.

Gallo, D., B., B.P., Morbiducci, U., Ye, Q., (Joyce), X.Y., Maryam, E., Damiaan, H., G., L.E., A., W.B., A., S.D., 2018. Segment-specific associations between local haemodynamic and imaging markers of early atherosclerosis at the carotid artery: an in vivo human study. Journal of The Royal Society Interface 15, 20180352.

Gallo, D., De Santis, G., Negri, F., Tresoldi, D., Ponzini, R., Massai, D., Deriu, M.A., Segers, P., Verhegghe, B., Rizzo, G., Morbiducci, U., 2012. On the Use of In Vivo Measured Flow Rates as Boundary Conditions for Image-Based Hemodynamic Models of the Human Aorta: Implications for Indicators of Abnormal Flow. Annals of Biomedical Engineering 40, 729–741.

Garcia, J., van der Palen, R.L.F., Bollache, E., Jarvis, K., Rose, M.J., Barker, A.J., Collins, J.D., Carr, J.C., Robinson, J., Rigsby, C.K., Markl, M., 2018. Distribution of blood flow velocity in the normal aorta: Effect of age and gender. Journal of Magnetic Resonance Imaging 47, 487–498.

Guala, A., Dux-Santoy, L., Teixido-Tura, G., Ruiz-Muñoz, A., Galian-Gay, L., Servato, M.L., Valente, F., Gutiérrez, L., González-Alujas, T., Johnson, K.M., 2022. Wall shear stress predicts aortic dilation in patients with bicuspid aortic valve. Cardiovascular Imaging 15, 46–56.

Gulan, U., Luthi, B., Holzner, M., Liberzon, A., Tsinober, A., Kinzelbach, W., 2014. Experimental

Investigation of the Influence of the Aortic Stiffness on Hemodynamics in the Ascending Aorta. IEEE Journal of Biomedical and Health Informatics 18, 1775–1780.

Jin, S., Oshinski, J., Giddens, D.P., 2003. Effects of Wall Motion and Compliance on Flow Patterns in the Ascending Aorta. Journal of Biomechanical Engineering 125, 347–354.

Kilner, P.J., Yang, G.Z., Mohiaddin, R.H., Firmin, D.N., Longmore, D.B., 1993. Helical and retrograde secondary flow patterns in the aortic arch studied by three-directional magnetic resonance velocity mapping. Circulation 88, 2235–2247.

Lantz, J., Dyverfeldt, P., Ebbers, T., 2014. Improving Blood Flow Simulations by Incorporating Measured Subject-Specific Wall Motion. Cardiovascular Engineering and Technology 5, 261–269.

Lantz, J., Gupta, V., Henriksson, L., Karlsson, M., Persson, A., Carlhäll, C.-J., Ebbers, T., 2019. Impact of Pulmonary Venous Inflow on Cardiac Flow Simulations: Comparison with In Vivo 4D Flow MRI. Annals of Biomedical Engineering 47, 413–424.

LeMaire, S.A., Russell, L., 2011. Epidemiology of thoracic aortic dissection. Nature Reviews Cardiology 8, 103–113.

Liu, X., Pu, F., Fan, Y., Deng, X., Li, D., Li, S., 2009. A numerical study on the flow of blood and the transport of LDL in the human aorta: the physiological significance of the helical flow in the aortic arch. American Journal of Physiology-Heart and Circulatory Physiology 297, H163–H170.

Liu, X., Sun, A., Fan, Y., Deng, X., 2015. Physiological significance of helical flow in the arterial system and its potential clinical applications. Annals of biomedical engineering 43, 3–15.

Markl, M., Draney, M.T., Hope, M.D., Levin, J.M., Chan, F.P., Alley, M.T., Pelc, N.J., Herfkens, R.J., 2004. Time-resolved 3-dimensional velocity mapping in the thoracic aorta: visualization of 3-directional blood flow patterns in healthy volunteers and patients. Journal of computer assisted tomography 28, 459–468.

Mazzi, V., Morbiducci, U., Calò, K., De Nisco, G., Lodi Rizzini, M., Torta, E., Caridi, G.C.A., Chiastra, C., Gallo, D., 2021. Wall Shear Stress Topological Skeleton Analysis in Cardiovascular Flows: Methods and Applications. Mathematics 9, 720.

Menut, M., Boussel, L., Escriva, X., Bou-Saïd, B., Walter-Le Berre, H., Marchesse, Y., Millon, A., Della Schiava, N., Lermusiaux, P., Tichy, J., 2018. Comparison between a generalized Newtonian model and a network-type multiscale model for hemodynamic behavior in the aortic arch: Validation with 4D MRI data for a case study. Journal of Biomechanics 73, 119–126.

Mirramezani, M., Shadden, S.C., 2022. Distributed lumped parameter modeling of blood flow in compliant vessels. Journal of Biomechanics 140, 111161.

Morbiducci, U., Gallo, D., Cristofanelli, S., Ponzini, R., Deriu, M.A., Rizzo, G., Steinman, D.A., 2015. A rational approach to defining principal axes of multidirectional wall shear stress in realistic vascular geometries, with application to the study of the influence of helical flow on wall shear stress directionality in aorta. Journal of biomechanics 48, 899–906.

Morbiducci, U., Ponzini, R., Gallo, D., Bignardi, C., Rizzo, G., 2013. Inflow boundary conditions for image-based computational hemodynamics: Impact of idealized versus measured velocity profiles in the human aorta. Journal of Biomechanics 46, 102–109.

Morbiducci, U., Ponzini, R., Grigioni, M., Redaelli, A., 2007. Helical flow as fluid dynamic signature for atherogenesis risk in aortocoronary bypass. A numeric study. Journal of biomechanics 40, 519–534.

Morbiducci, U., Ponzini, R., Rizzo, G., Cadioli, M., Esposito, A., De Cobelli, F., Del Maschio, A., Montevecchi, F.M., Redaelli, A., 2009. In vivo quantification of helical blood flow in human aorta by time-resolved three-dimensional cine phase contrast magnetic resonance imaging. Annals of biomedical engineering 37, 516–531.

Morbiducci, U., Ponzini, R., Rizzo, G., Cadioli, M., Esposito, A., Montevecchi, F.M., Redaelli, A., 2011. Mechanistic insight into the physiological relevance of helical blood flow in the human aorta: an in vivo study. Biomechanics and Modeling in Mechanobiology 10, 339–355.

Oechtering, T.H., Sieren, M.M., Hunold, P., Hennemuth, A., Huellebrand, M., Scharfschwerdt, M., Richardt, D., Sievers, H.-H., Barkhausen, J., Frydrychowicz, A., 2020. Time-resolved 3-dimensional magnetic resonance phase contrast imaging (4D Flow MRI) reveals altered blood flow patterns in the ascending aorta of patients with valve-sparing aortic root replacement. The Journal of Thoracic and Cardiovascular Surgery 159, 798-810.e1.

Reymond, P., Crosetto, P., Deparis, S., Quarteroni, A., Stergiopulos, N., 2013. Physiological simulation of blood flow in the aorta: Comparison of hemodynamic indices as predicted by 3-D FSI, 3-D rigid wall and 1-D models. Medical Engineering & Physics 35, 784–791.

Romarowski, R.M., Lefieux, A., Morganti, S., Veneziani, A., Auricchio, F., 2018. Patient-specific CFD modelling in the thoracic aorta with PC-MRI–based boundary conditions: A least-square three-element Windkessel approach. International Journal for Numerical Methods in Biomedical Engineering 34, e3134.

Sengupta, P.P., Tajik, A.J., Chandrasekaran, K., Khandheria, B.K., 2008. Twist Mechanics of the Left Ventricle: Principles and Application. JACC: Cardiovascular Imaging 1, 366–376.

Shadden, S.C., Taylor, C.A., 2008. Characterization of coherent structures in the cardiovascular system. Annals of biomedical engineering 36, 1152–1162.

Stokes, C., Bonfanti, M., Li, Z., Xiong, J., Chen, D., Balabani, S., Díaz-Zuccarini, V., 2021. A novel MRI-based data fusion methodology for efficient, personalised, compliant simulations of aortic haemodynamics. Journal of Biomechanics 129, 110793.

Stonebridge, P.A., Suttie, S.A., Ross, R., Dick, J., 2016. Spiral Laminar Flow: a Survey of a Three-Dimensional Arterial Flow Pattern in a Group of Volunteers. European journal of vascular and endovascular surgery : the official journal of the European Society for Vascular Surgery 52, 674–680.

Thiene, G., Basso, C., Della Barbera, M., 2021. Pathology of the Aorta and Aorta as Homograft. Journal of Cardiovascular Development and Disease 8, 76.

Torii, R., Keegan, J., Wood, N.B., Dowsey, A.W., Hughes, A.D., Yang, G.-Z., Firmin, D.N., Thom, S.A.M., Xu, X.Y., 2010. MR Image-Based Geometric and Hemodynamic Investigation of the Right Coronary Artery with Dynamic Vessel Motion. Annals of Biomedical Engineering 38, 2606–2620.

Vignali, E., Gasparotti, E., Celi, S., Avril, S., 2021. Fully-Coupled FSI Computational Analyses in the Ascending Thoracic Aorta Using Patient-Specific Conditions and Anisotropic Material Properties. Frontiers in Physiology 12, 732561.

Yearwood, T.L., Chandran, K.B., 1982. Physiological pulsatile flow experiments in a model of the human aortic arch. Journal of Biomechanics 15, 683–704.

Youssefi, P., Gomez, A., Arthurs, C., Sharma, R., Jahangiri, M., Alberto Figueroa, C., 2018. Impact of Patient-Specific Inflow Velocity Profile on Hemodynamics of the Thoracic Aorta. Journal of Biomechanical Engineering 140.

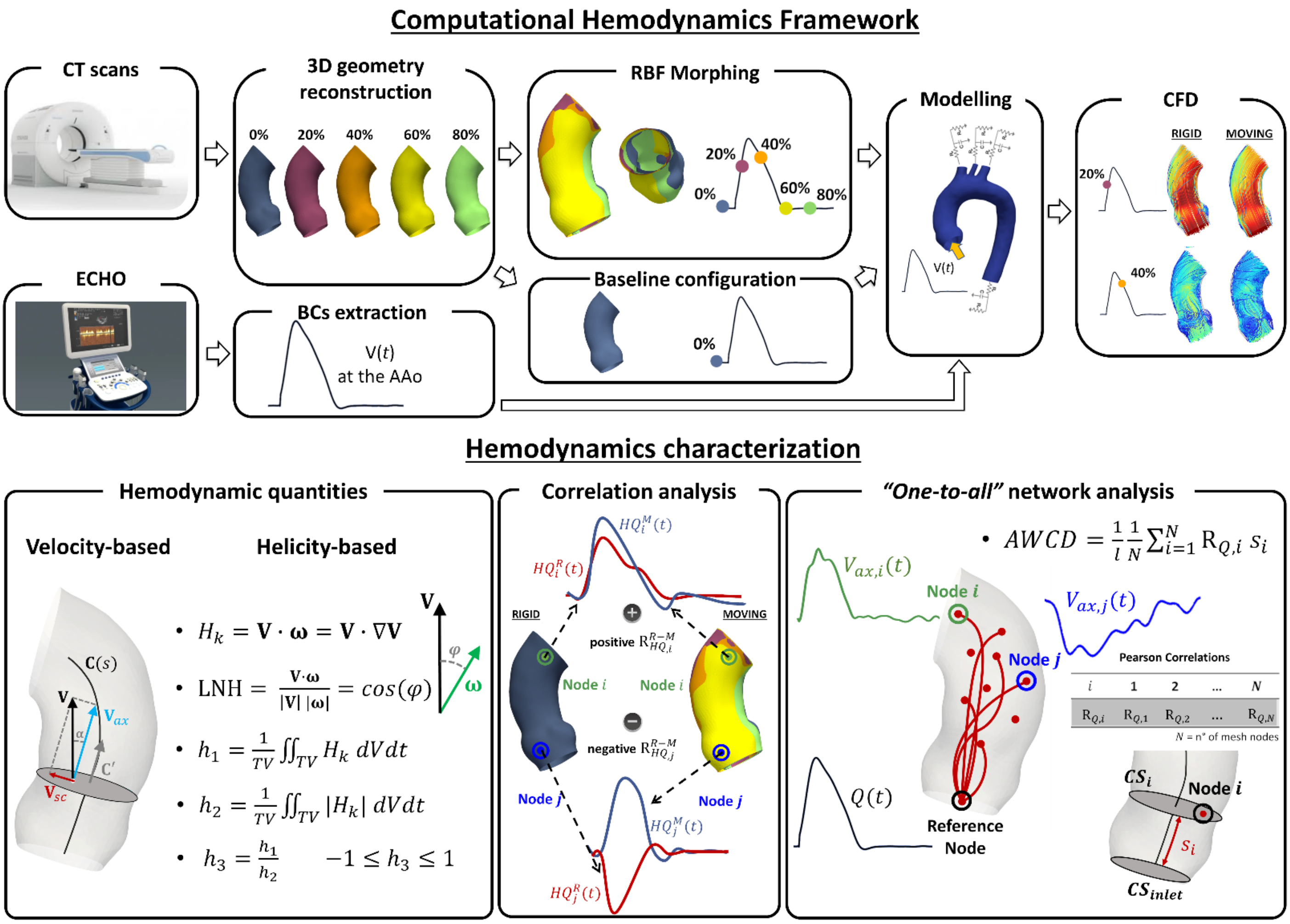

Fig. 1. Schematic diagram of the methodology applied to investigate the impact that aortic wall displacements have on large-scale flow coherence in the AAo. Medical imaging is used to reconstruct the aortic geometry along the cardiac cycle and to extract subject-specific boundary conditions applied to perform CFD simulations (upper panel). The impact of AAo wall displacements is investigated in terms of velocity- and helicity-based hemodynamic quantities, through a correlation analysis and a *"one-to-all"* network approach (lower panel).

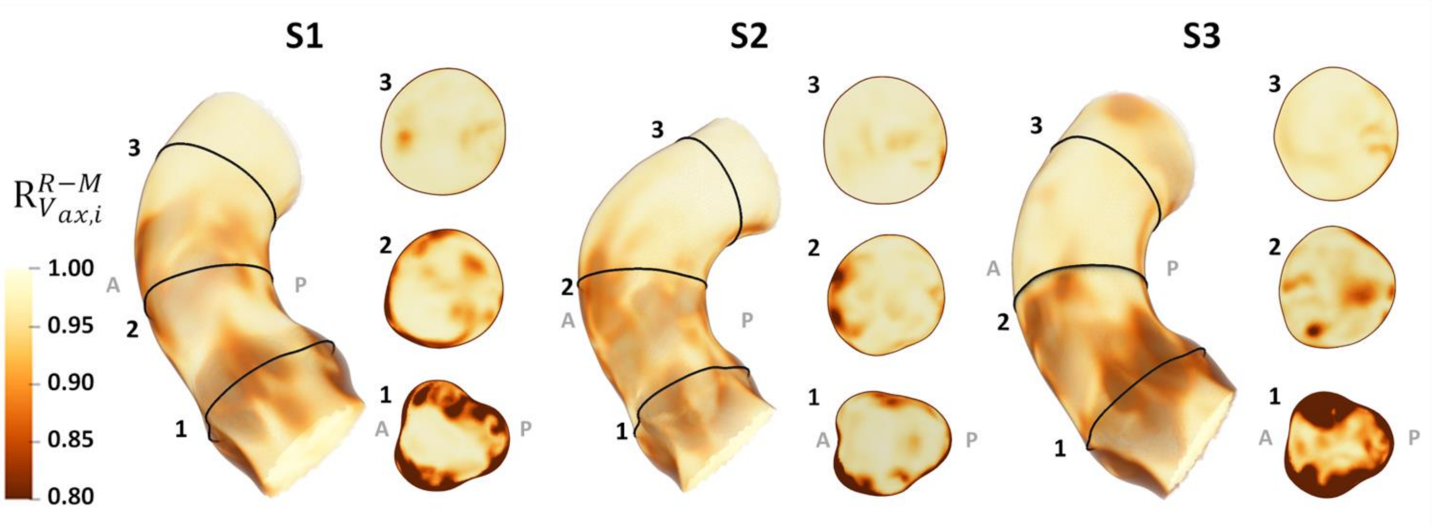

Fig. 2. Impact of aortic motion on the spatiotemporal similarity of axial flow in the AAo: volumetric maps of correlation coefficients $R^{R-M}_{V_{ax,i}}$ between the $V_{ax,i}(t)$ waveforms at corresponding nodes of the rigid- and moving-wall models. Maps at three cross-sections along the AAo are also displayed.

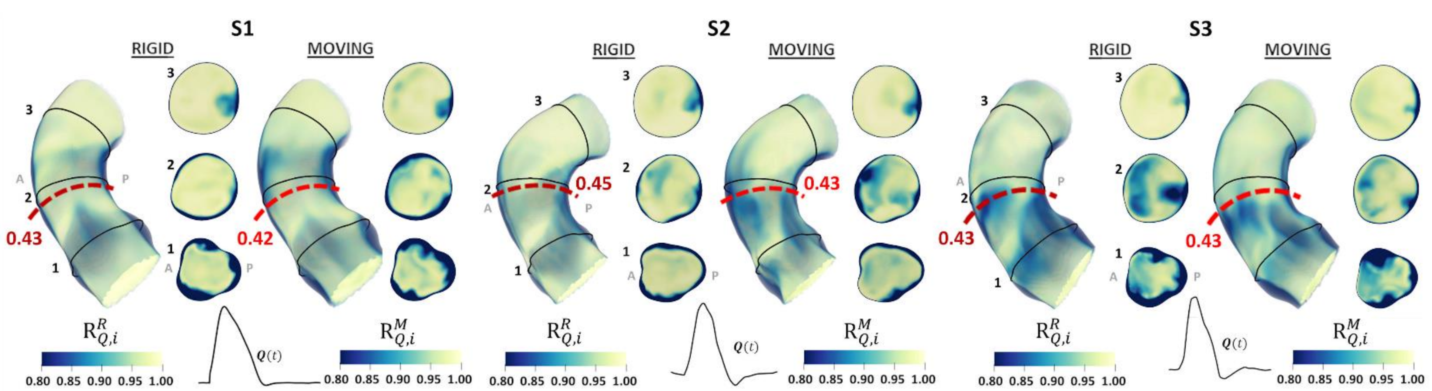

Fig. 3. *"One-to-all"* network analysis to evaluate the impact of wall displacements on the spatiotemporal similarity of axial velocity waveforms with the blood flow rate waveform at the AAo inlet section: volume maps of the correlation coefficients between $Q(t)$ and $V_{ax,i}(t)$ waveforms in the rigid- ($R^R_{Q,i}$) and in the moving-wall ($R^M_{Q,i}$) models. The $AWCD$ values measuring the anatomical length of persistence of the correlation between $Q(t)$ and $V_{ax,i}(t)$ in the AAo are reported in red. Maps at three cross-sections along the AAo are also displayed.

This article has been accepted for publication in the Journal of Biomechanics. This is the author's preprint version.
Citation information: DOI 10.1016/j.jbiomech.2023.111620

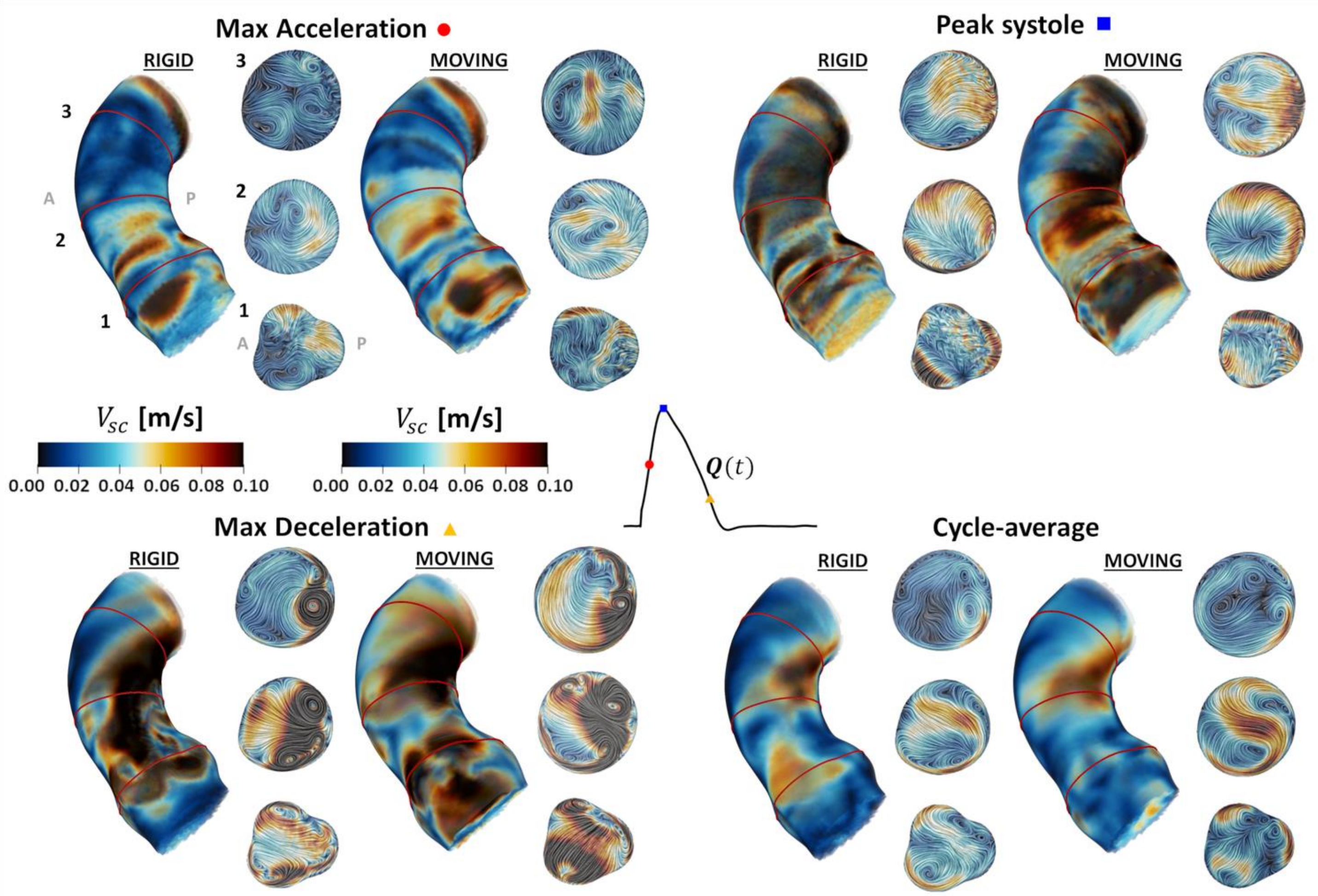

Fig. 4. Impact of aortic motion on secondary flows in the AAo: volume maps of the secondary velocity magnitude $|V_{sc}|$ cycle-averaged and at three different phases of the cardiac cycle (peak systole, maximum flow acceleration and deceleration), in the rigid- and moving-wall models for the explanatory subject S1. Secondary flows at three cross-sections along the AAo are also displayed.

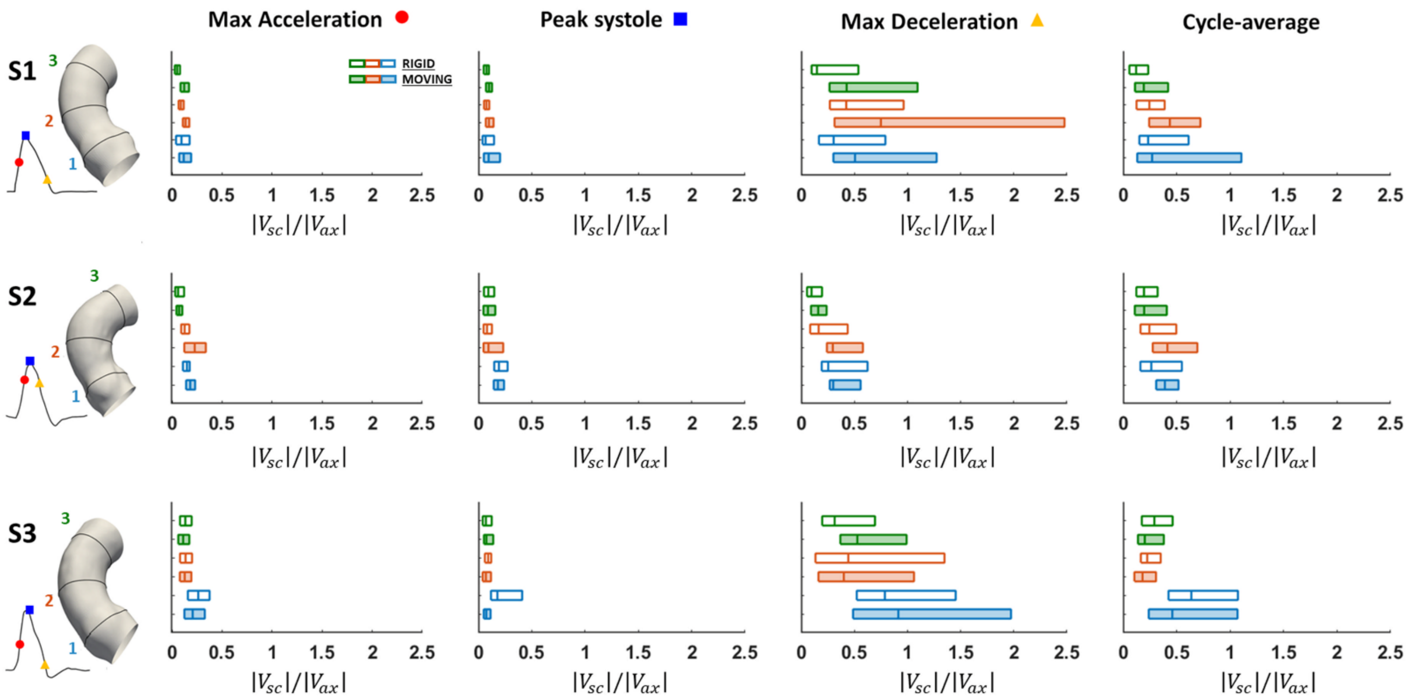

565 **Fig. 5.** Boxplots of $|V_{sc}|/|V_{ax}|$ values cycle-averaged and at three different phases of the cardiac cycle
566 (peak systole, maximum flow acceleration and deceleration), at three cross-sections along the AAo
567 in the rigid- and moving-wall models.

568

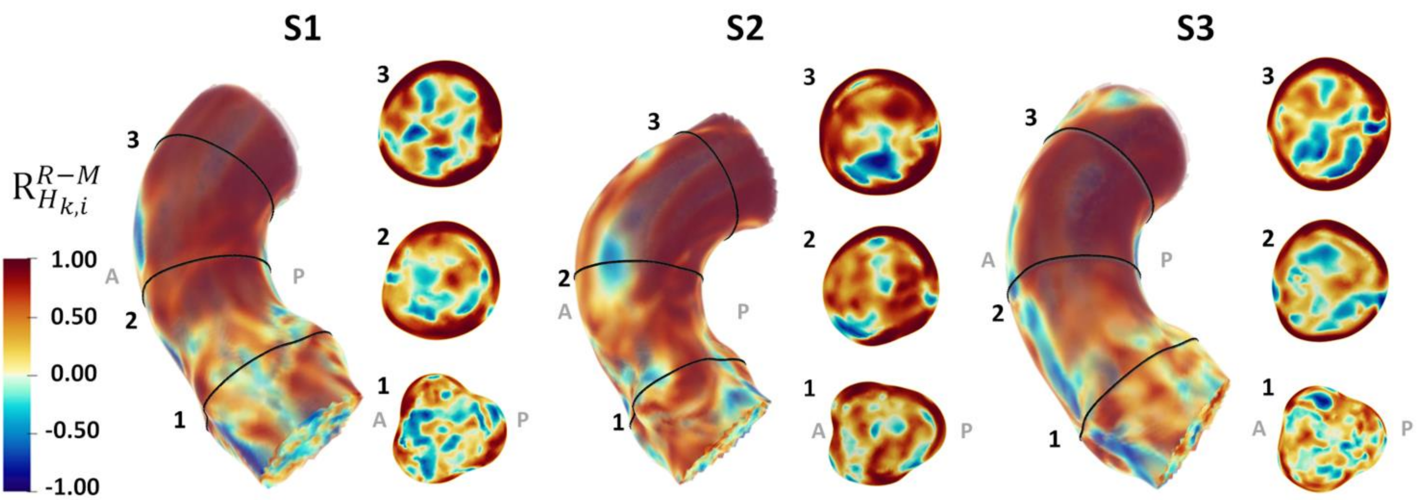

569 **Fig. 6.** Impact of aortic motion on the spatiotemporal similarity of helical flow in the AAo: volume
570 maps of the correlation coefficients $R_{H_{k,i}}^{R-M}$ between the $H_{k,i}(t)$ waveforms at corresponding nodes of
571 the rigid- and moving-wall models. Maps at three cross-sections along the AAo are also displayed.

572

This article has been accepted for publication in the Journal of Biomechanics. This is the author's preprint version.
Citation information: DOI 10.1016/j.jbiomech.2023.111620

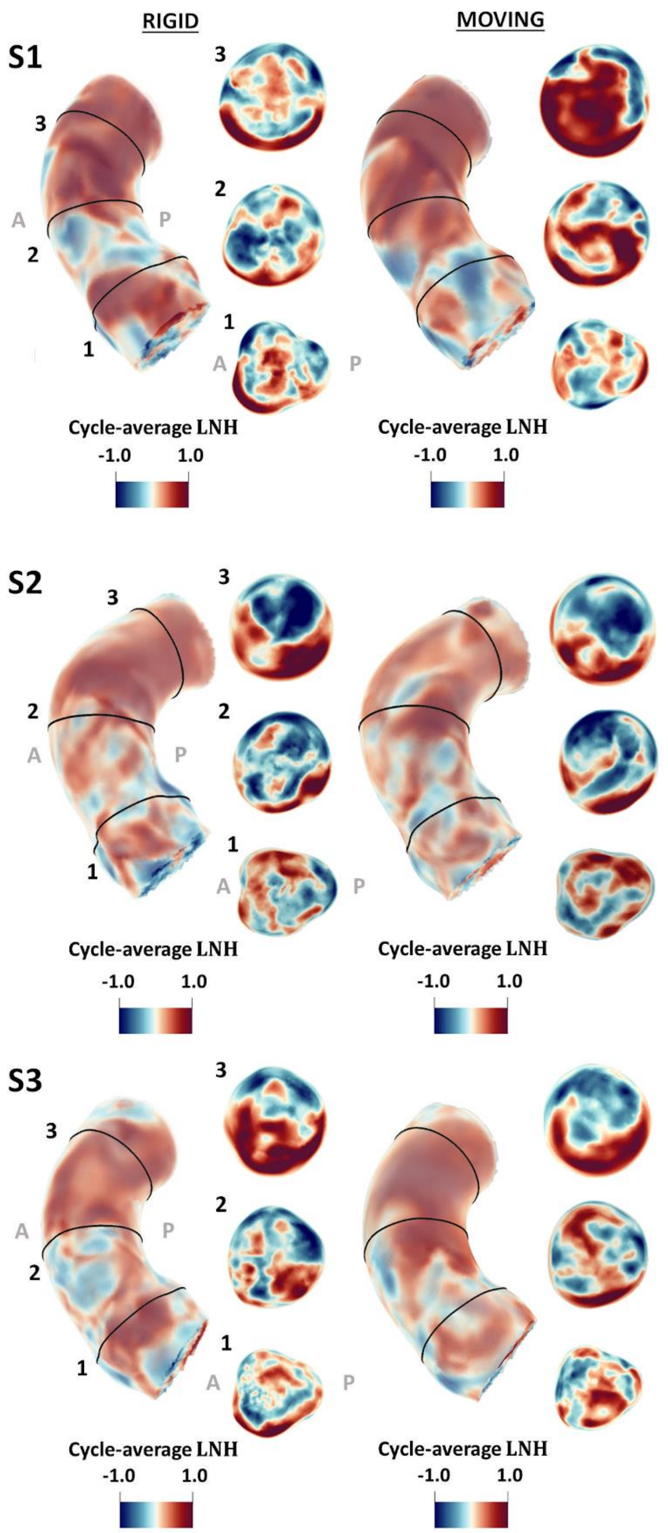

Fig. 7. Impact of aortic motion on helical flow topological features in the AAo: volume maps of cycle-average LNH in the rigid- and moving-wall models. Positive (red) and negative (blue) LNH values indicate counter-rotating flow structures.

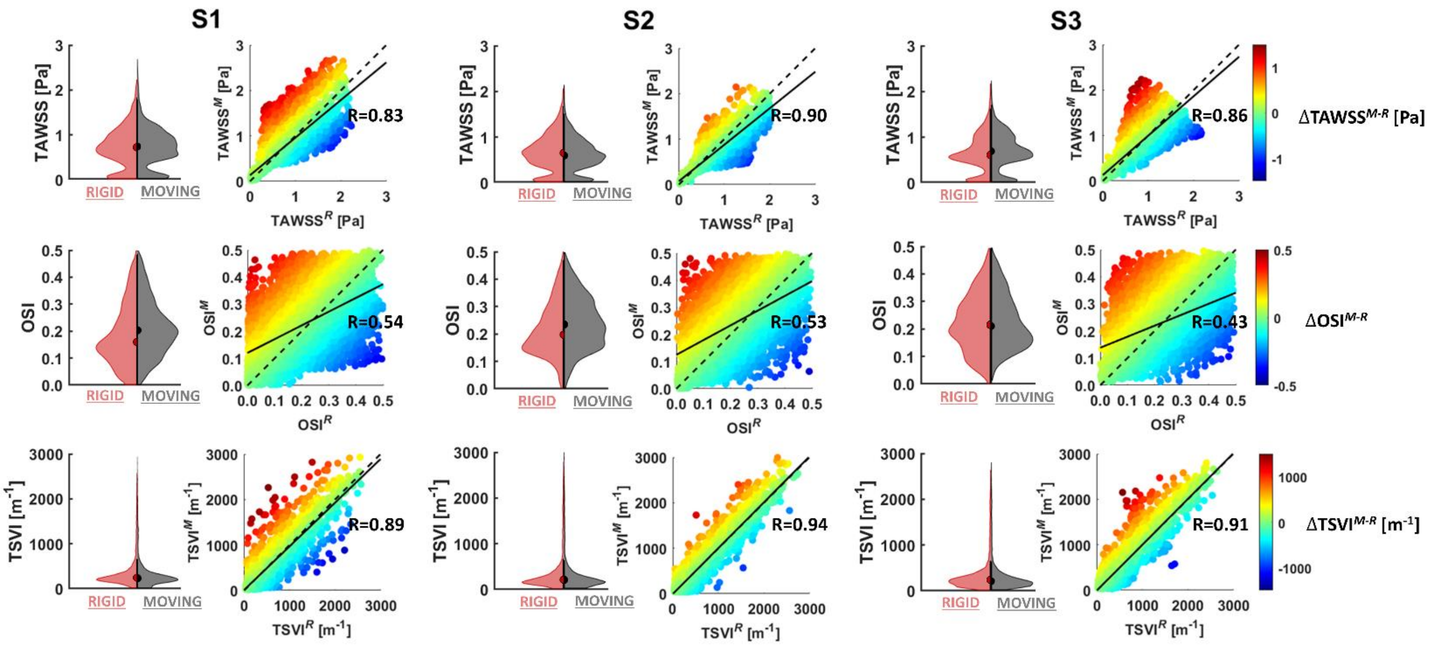

Fig. 8. Impact of aortic motion on wall shear stress in the AAo: violin plots and scatter plots of TAWSS, OSI and TSVI in the rigid- and moving-wall models. Colormap in the scatter plots indicates the absolute difference between the moving- and the rigid-wall case in the nodal values of the investigated WSS-based quantities. The identity line as well as the regression line with the Pearson correlation coefficient R are also displayed.

Investigated WSS-based quantities	
Time-averaged Wall Shear Stress (TAWSS)	$\mathrm{TAWSS} = \frac{1}{T}\int_0^T \lvert\mathbf{WSS}\rvert\, dt$
Oscillatory Shear Index (OSI)	$\mathrm{OSI} = 0.5\left[1 - \left(\frac{\left\lvert\int_0^T \mathbf{WSS}\ dt\right\rvert}{\int_0^T \lvert\mathbf{WSS}\rvert\, dt}\right)\right]$
Topological Shear Variation Index (TSVI)	$\mathrm{TSVI} = \left\{\frac{1}{T}\int_0^T \left[\nabla\cdot(\mathbf{WSS}_{\boldsymbol{u}}) - \overline{\nabla\cdot(\mathbf{WSS}_{\boldsymbol{u}})}\right]^2 dt\right\}^{1/2}$

Table 1 Investigated WSS-based quantities: **WSS** is the time-varying wall shear stress vector; T is the cardiac cycle duration; $\mathbf{WSS_u}$ is the WSS unit vector; $\nabla\cdot(\mathbf{WSS_u})$ is the divergence of the WSS unit vector field; the overbar denotes a cycle-average quantity.

	S1		S2		S3	
	Rigid	**Moving**	**Rigid**	**Moving**	**Rigid**	**Moving**
h_1 [m s^{-2}]	0.15	0.46	-0.35	-0.36	-0.09	0.03
h_2 [m s^{-2}]	3.67	3.76	3.76	3.48	3.91	3.22
h_3	0.04	0.12	-0.09	-0.10	-0.02	0.01

587 **Table 2** Values of the helicity-based quantities h_i for the rigid- and moving-wall models.

588